Flexible All-Solid-State Asymmetric Supercapacitors Based on Free-Standing Carbon Nanotube/Graphene and Mn$_3$O$_4$ Nanoparticle/Graphene Paper Electrodes

Hongcai Gao, Fei Xiao, Chi Bun Ching, and Hongwei Duan*

School of Chemical and Biomedical Engineering, Nanyang Technological University, 70 Nanyang Drive, Singapore 637457

S *Supporting Information*

ABSTRACT: We report the design of all-solid-state asymmetric supercapacitors based on free-standing carbon nanotube/graphene (CNTG) and Mn$_3$O$_4$ nanoparticles/graphene (MG) paper electrodes with a polymer gel electrolyte of potassium polyacrylate/KCl. The composite paper electrodes with carbon nanotubes or Mn$_3$O$_4$ nanoparticles uniformly intercalated between the graphene nanosheets exhibited excellent mechanical stability, greatly improved active surface areas, and enhanced ion transportation, in comparison with the pristine graphene paper. The combination of the two paper electrodes with the polymer gel electrolyte endowed our asymmetric supercapacitor of CNTG//MG an increased cell voltage of 1.8 V, a stable cycling performance (capacitance retention of 86.0% after 10 000 continuous charge/discharge cycles), more than 2-fold increase of energy density (32.7 Wh/kg) compared with the symmetric supercapacitors, and importantly a distinguished mechanical flexibility.

KEYWORDS: *energy storage, graphene paper, all-solid-state, asymmetric supercapacitor*
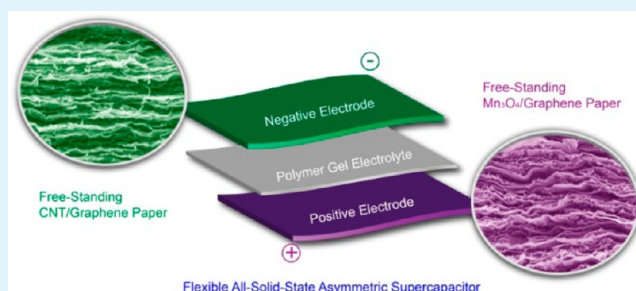
1. INTRODUCTION

Flexible energy storage devices that can function under considerable physical deformation have attracted increasing attention for a wide range of applications in portable electronics, paper-like personal gadgets, and miniature biomedical devices.[1−3] The development of supercapacitors using polymer gel electrolytes represents a promising strategy toward safe, flexible, light-weighted, and all-solid-state energy storage devices with a unique set of characteristics such as high power density, fast charge/discharge rate, and excellent cycling stability.[4−9] In particular, asymmetric supercapacitors (ASC) with electrode materials working in well-separated potential windows in the same electrolyte can extend the cell voltage of aqueous electrolytes beyond the thermodynamic limit of 1.2 V and thus significantly improve the energy density.[10−13] The design of flexible ASC necessitates the advancement of free-standing paper-like electrodes, which can significantly simplify cell packing by eliminating inactive ingredients such as binders and current collectors and thus improve the overall performance when the total mass of the device is taken into account.[14−16]

Carbon materials and transition metal oxides are commonly employed as negative and positive electrodes in asymmetric supercapacitors because of their complementary working potential windows.[17−19] Different challenges are currently present for these two types of electrode materials when used in flexible ASC. Among the diverse types of carbon materials, graphene holds great promise in supercapacitor applications

because of the unprecedented combination of large surface area, superior electrical conductivity, and flexibility.[20−24] However, the strong van der Waals interaction between their hydrophobic basal planes drives the restacking and aggregation of the nanosheets when forming free-standing paper electrodes, leading to greatly reduced surface areas.[25,26] On the other hand, transition metal oxides such as manganese oxides (i.e., MnO$_2$ and Mn$_3$O$_4$),[27−29] although exhibiting high energy density, have shown limited power density due to their poor electrical conductivity. In addition, it is also challenging to process transition metal oxides into flexible electrodes without adding inactive supporting materials. In response to these significant challenges, innovative graphene structures have been developed to minimize the restacking-induced surface area loss, such as holey graphene,[30,31] curved and crumpled graphene,[32] and 3D interconnected graphene networks;[33,34] great efforts have also been made to structurally integrate transition metal oxides with conductive carbon substrates, leading to hybrid electrodes with improved electrical conductivity.[35−37] Nevertheless, limited success has been achieved in producing flexible ASC with free-standing electrodes featuring optimal electrochemical properties and mechanical strength.[38,39]

Here, we report the design of all-solid-state ASC based on polymer gel electrolytes and free-standing paper electrodes with

Scheme 1. Illustration of the Fabrication Process for Flexible All-Solid-State Asymmetric Supercapacitors Based on Polymer Gel Electrolyte and Free-Standing CNTG and MG Paper Electrodes
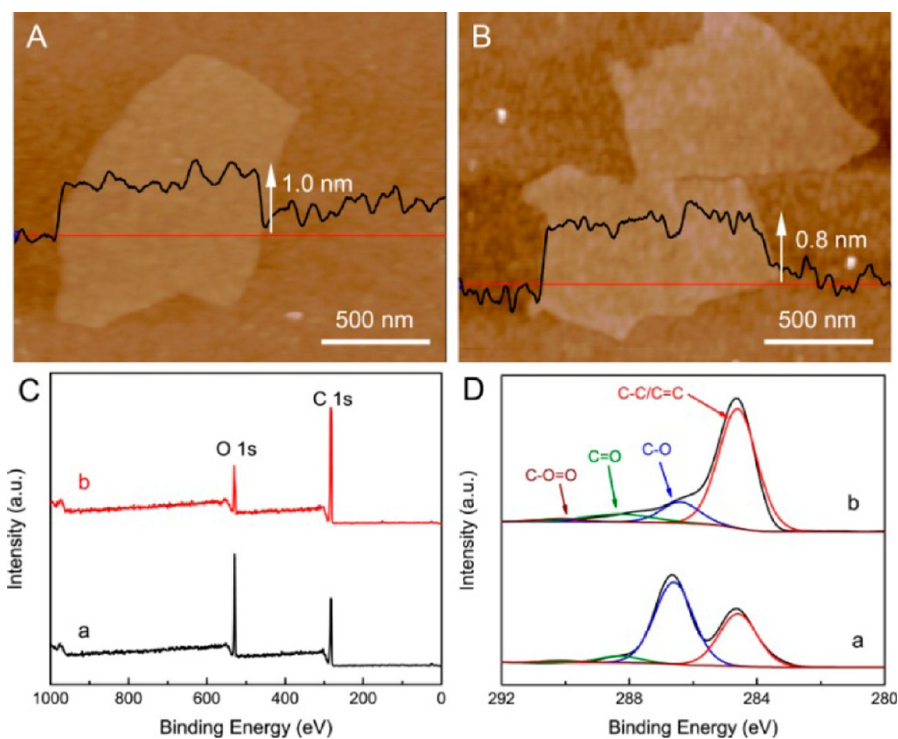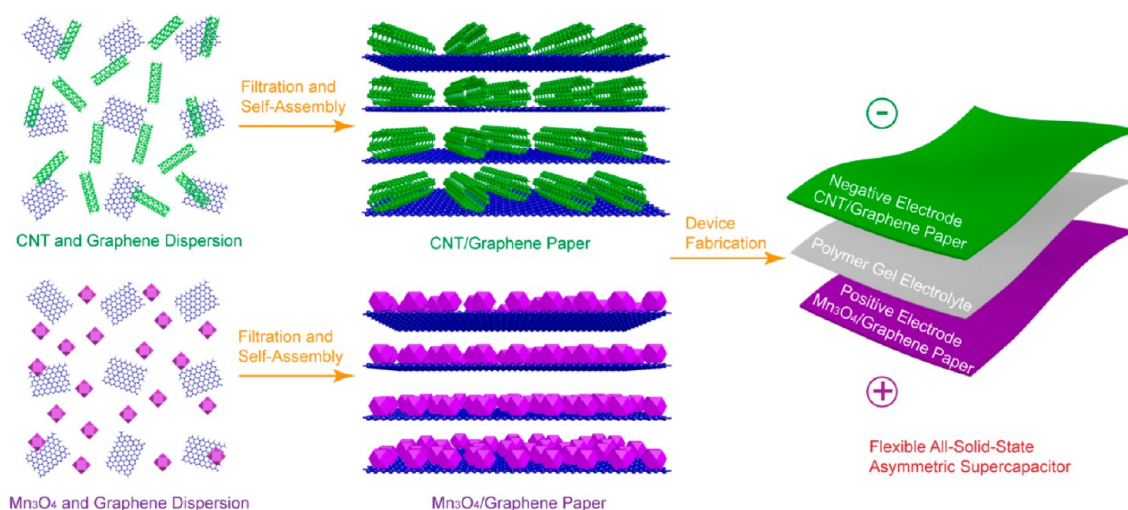

Figure 1. AFM images and height profiles of (A) GO and (B) rGO spin-coated on silicon wafers. (C) XPS survey spectra for GO (a) and rGO (b). (D) High-resolution XPS spectra of C 1s for GO (a) and rGO (b).

carbon nanotubes (CNTs) and Mn_3O_4 nanoparticles structurally intercalated between the graphene layers (Scheme 1). Taking advantage of the colloidal nature of graphene, CNTs, and Mn_3O_4 nanoparticles, our results have shown that multilayered structures of the two paper electrodes were readily formed in the flow-directed self-assembly process and effectively addressed the above-mentioned problems associated with graphene-based negative electrodes and transition metal oxide-derived positive electrodes. The integration of free-standing paper electrodes with polymer gel electrolytes led to flexible ASC exhibiting concurrent high energy density and power density, remarkable rate capability, excellent cycling stability, and especially distinguished mechanical flexibility.

2. EXPERIMENTAL SECTION

2.1. Preparation of Samples. Graphene oxides (GO) were synthesized from graphite power according to the modified Hummers' method.[40,41] Reduced graphene oxides (rGO) were prepared by hydrothermal reduction of GO (0.1 mg/mL with pH adjusted to 10) at 180 °C for 12 h.[42,43] CNTs were purified and functionalized by refluxing in concentrated HNO_3 for 6 h to introduce carboxylic groups.[44] Mn_3O_4 nanoparticles were synthesized by reacting NaOH (0.25 M, 60 mL) with $Mn(CH_3COO)_2 \cdot 4H_2O$ (0.08 M, 90 mL) containing polyethylene glycol (30 mg) to obtain precipitates, and stirring was maintained for 3 h afterward.[45] Free-standing CNT/rGO (CNTG) and Mn_3O_4 nanoparticles/rGO (MG) papers were prepared by filtrating the mixtures of rGO with CNTs or Mn_3O_4 nanoparticles through cellulose acetate membrane filters, followed by washing, air drying, and peeling off from the filters.

2.2. Materials Characterization. The morphology of the samples was investigated by atomic force microscope (AFM, Asylum Research) and field-emission scanning electron microscopy (SEM, JSM-6700F). AFM samples were prepared by spin-coating GO, rGO, or CNTs dispersions on silicon wafers with a 300 nm SiO_2 top layer and then characterized with a silicon cantilever operating in tapping mode. Zeta potentials of rGO, CNTs, and Mn_3O_4 nanoparticles suspensions were measured at room temperature on ZetaPALS Zeta Potential Analyzer (Brookhaven Instruments Corporation). X-ray diffraction (XRD) patterns were collected with a Bruker AXS D8 X-ray diffractometer equipped with monochromatized Cu Kα radiation (λ = 1.54056 Å, 40 kV, and 20 mA). X-ray photoelectron spectroscopy (XPS) measurements were performed on a Kratos-Axis spectrometer with monochromatic Al Kα (1486.71 eV) X-ray radiation (15 kV and 10 mA) and a hemispherical electron energy analyzer. Curve fitting and background subtraction were accomplished using Casa XPS software. The tensile behaviors of rGO paper-based samples were measured on an Instron Microforce Tester at a loading rate of 0.05 mm/min. Quantachrome Autosorb 6B system was used to characterize the specific surface areas and pore structures of the electrode materials using nitrogen sorption under 77.4 K. The specific surface areas and pore size distributions of the electrode materials were calculated by Brunauer−Emmett−Teller (BET) and Barrett−Joyner−Halenda (BJH) methods, respectively.

2.3. Electrochemical Measurements. CNTG, MG, and rGO papers were cut into pieces and directly used as electrodes to fabricate symmetric or asymmetric supercapacitors. Potassium polyacrylate (PAAK)/KCl gel electrolyte was prepared by adding 1.0 g of PAAK into 10 mL of KCl solution (1.0 M).[46] Two strips of the paper electrodes were immersed into the PAAK/KCl solution for 30 min. After evaporation of excess water, the two paper electrodes were assembled together under pressing to fabricate all-solid-state supercapacitors. The specific capacitance (C_t) of a supercapacitor cell was calculated from the equation of $C_t = I\Delta t/m\Delta V$, where I is the discharge current, Δt is the discharge time, m is the total mass of active materials in two electrodes, and ΔV is the voltage drop upon discharge (excluding IR drop). In symmetric supercapacitors, the specific capacitance (C_{sc}) of the electrodes (CNTG or MG) was calculated according to $C_{sc} = 4C_t$. The energy density (E) and power density (P) of a supercapacitor cell in the Ragone plots were calculated following the equations of $E = 1/2C_t\Delta V^2$ and $P = E/\Delta t$, respectively.[47−49]

3. RESULTS AND DISCUSSION

3.1. Negative Electrodes. Reduced graphene oxides (rGO) were prepared by hydrothermal reduction of GO solutions at 180 °C for 12 h.[42,43] Compared with GO, the thickness of rGO decreases to about 0.8 nm (Figure 1A,B), matching well with that of single layered rGO reported previously,[50] and rGO has a higher carbon to oxygen ratio (8.0) than GO (2.0) (Figure 1C,D), which is expected to improve the electrical conductivity of rGO nanosheets. CNTs with a diameter of about 2.0 nm (Figure S1A, Supporting Information) were purified and functionalized by refluxing in concentrated HNO_3 to introduce carboxylic groups.[44] Resulting from the deprotonation of carboxylic acid groups,[51] both rGO and CNTs are negatively charged with zeta potentials of −57 and −39 mV and can form homogeneous dispersions after mild sonication of their mixtures.

Free-standing and flexible CNT/rGO (CNTG) papers with CNTs mass ratio of 20% (CNTG-20) and 40% (CNTG-40) were successfully prepared after filtration of their mixtures through cellulose acetate membranes (Figure 2A,B). In the hybrid CNTG papers, CNTs are uniformly incorporated between rGO nanosheets to form sandwiched structures (Figure 2D,E,F) and tend to assemble into bundles with diameter of about 20 nm after filtration and drying (Figure S1B, Supporting Information). The specific surface areas of CNTG-
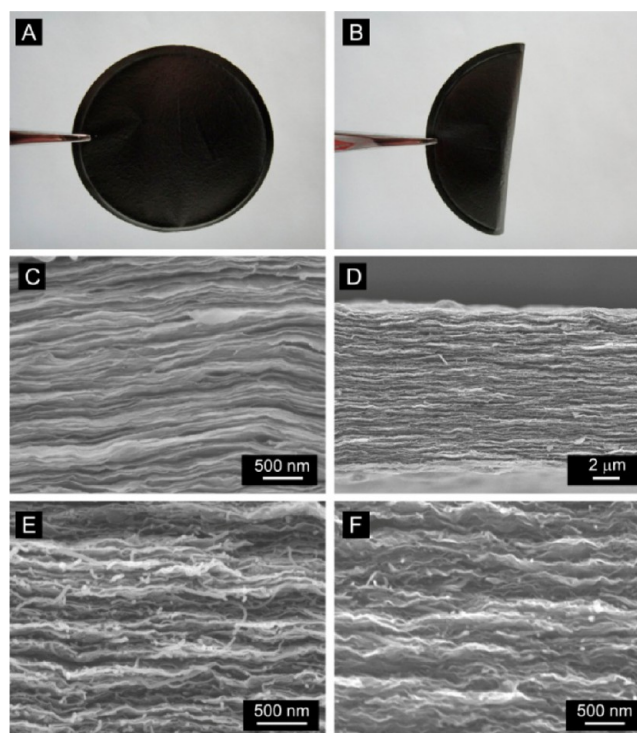

Figure 2. (A) Photograph of CNTG-40 paper with a diameter of 4 cm. (B) Photograph shows the free-standing CNTG-40 paper is flexible enough to be folded up. (C) Cross-section SEM image of rGO paper. (D and E) Cross-section SEM images of CNTG-40 paper with low and high magnifications. (F) Cross-section SEM image of CNTG-20 paper.
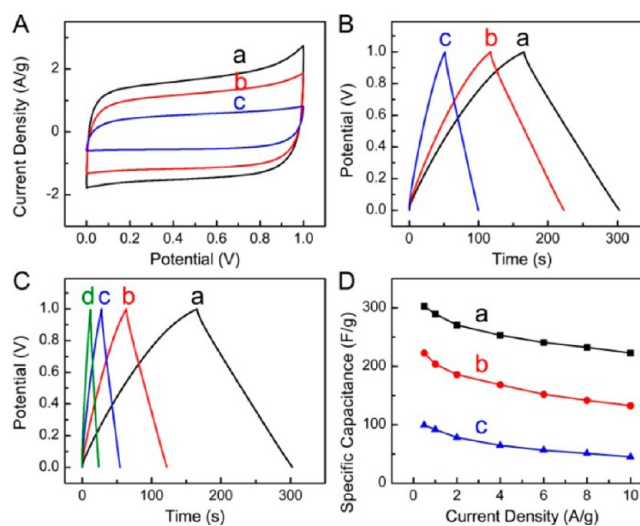

Figure 3. (A) Cyclic voltammograms of CNTG-40 (a), CNTG-20 (b), and rGO (c) papers at a scan rate of 20 mV/s. (B) Galvanostatic charge/discharge curves of CNTG-40 (a), CNTG-20 (b), and rGO (c) papers at a current density of 0.5 A/g. (C) Galvanostatic charge/discharge curves of CNTG-40 paper at current densities of 0.5 (a), 1 (b), 2 (c), and 4 (d) A/g. (D) Specific capacitance of CNTG-40 (a), CNTG-20 (b), and rGO (c) papers as a function of discharge current densities.

20 and CNTG-40 were 130.7 and 197.6 m^2/g, with their pore size centered at around 3.0 nm (Figure S2, Supporting Information). In contrast, rGO paper exhibits compact layered structures (Figure 2C), with specific surface area of 72.5 m^2/g.
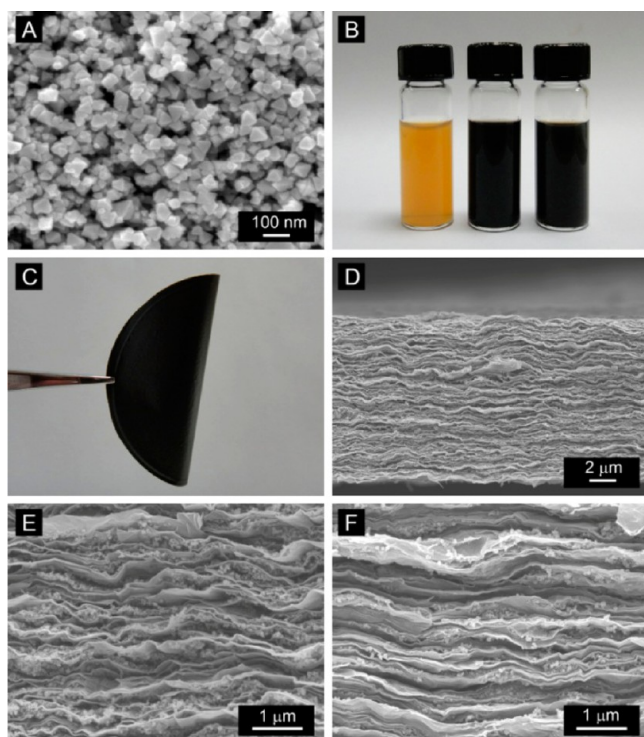
Figure 4. (A) SEM image of Mn₃O₄ nanoparticles. (B) Photographs of aqueous dispersions of Mn_3O_4 nanoparticles, rGO, and their mixture with a mass ratio of 1:1 (from left to right). (C) Photograph of MG-50 paper with a diameter of 4 cm and flexible enough to be folded up. (D and E) Cross-section SEM images of MG-50 paper with low and high magnifications. (F) Cross-section SEM image of MG-25 paper.
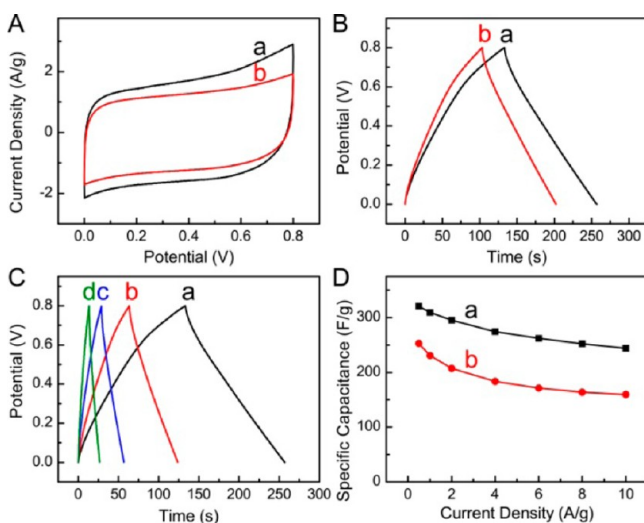

Figure 5. (A) Cyclic voltammograms of MG-50 (a) and MG-25 (b) papers at scan rate of 20 mV/s. (B) Galvanostatic charge/discharge curves of MG-50 (a) and MG-25 papers (b) at a current density of 0.5 A/g. (C) Galvanostatic charge/discharge curves of MG-50 paper at current densities of 0.5 (a), 1 (b), 2 (c), and 4 (d) A/g. (D) Specific capacitance of MG-50 (a) and MG-25 (b) papers as a function of discharge current densities.

Apparently, the incorporation of CNTs into CNTG can minimize the restacking and aggregation of rGO nanosheets, and as a result, more electrolyte-accessible surface areas become available, which is expected to facilitate the diffusion and movement of electrolyte ions into the interior of the
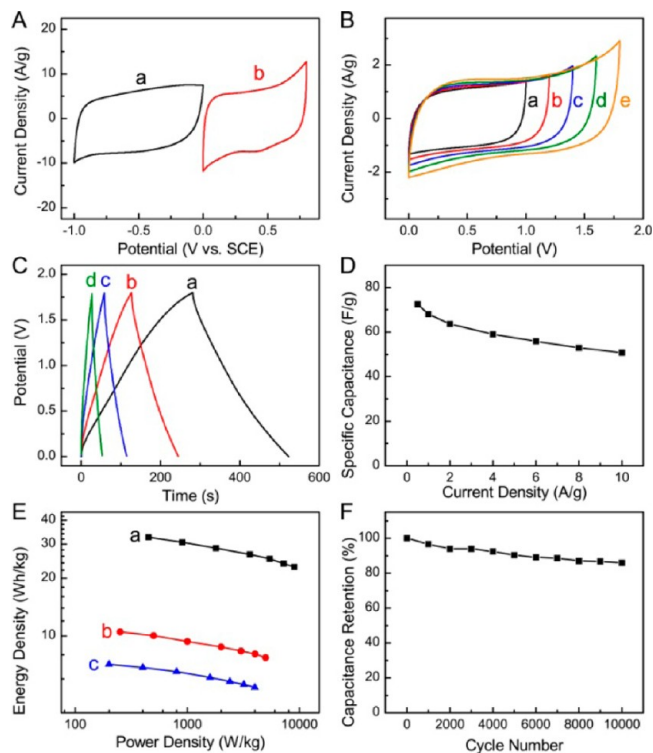

Figure 6. (A) Cyclic voltammograms of CNTG-40 (a) and MG-50 (b) in three-electrode systems. (B) Cyclic voltammograms of CNTG-40//MG-50 at cell voltages of 1.0 (a), 1.2 (b), 1.4 (c), 1.6 (d), and 1.8 (e) V. (C) Galvanostatic charge/discharge curves CNTG-40//MG-50 at current densities of 0.5 (a), 1 (b), 2 (c), and 4 (d) A/g. (D) Specific capacitance of CNTG-40//MG-50 as a function of current densities. (E) Ragone plots of CNTG-40//MG-50 (a), CNTG-40//CNTG-40 (b), and MG-50//MG-50 (c). (F) Cycling behavior of CNTG-40//MG-50 with a cell voltage of 1.8 V at a scan rate of 50 mV/s.

electrodes.[52−54] Interestingly, the tensile strengths of CNTG-20 and CNTG-40 increased to 68.2 and 46.7 MPa relative to that of the pristine rGO paper (41.7 MPa) (Figure S3A, Supporting Information). We reason that CNTs can bridge rGO nanosheets together through strong $\pi-\pi$ interactions between CNTs and rGO nanosheets and thus reinforce the mechanical strength of CNTG papers.[55]

The free-standing rGO and CNTG papers were directly used as electrodes to fabricate all-solid-state symmetric supercapacitors with the polymer gel electrolyte of PAAK/KCl. The nearly rectangular cyclic voltammetry (CV) curves (Figure 3A) and the linear charge/discharge profiles (Figure 3B,C) are the typical characteristics of electric double-layer capacitors. From the charge/discharge curves, the specific capacitance (C_{sc}) of rGO paper was calculated to be 99.7 F/g at the current density of 0.5 A/g, which is lower than rGO powder (∼200 F/g) reported previously.[56,57] We reason that, in the pristine rGO paper, the strong $\pi-\pi$ interactions between the basal planes lead to the restacking of graphene nanosheets and therefore induce the significant loss of its specific surface areas. After the incorporation of CNTs into rGO paper, the specific capacitances (C_{sc}) of CNTG-40 and CNTG-20 were increased to be 302.9 and 212.9 F/g, respectively, at the same current density. Impressively, compared with rGO paper, CNTG papers not only exhibit higher specific capacitances but also retain them well even at high current densities. Specifically, the specific capacitance of CNTG-40 can reach 220.8 F/g at a
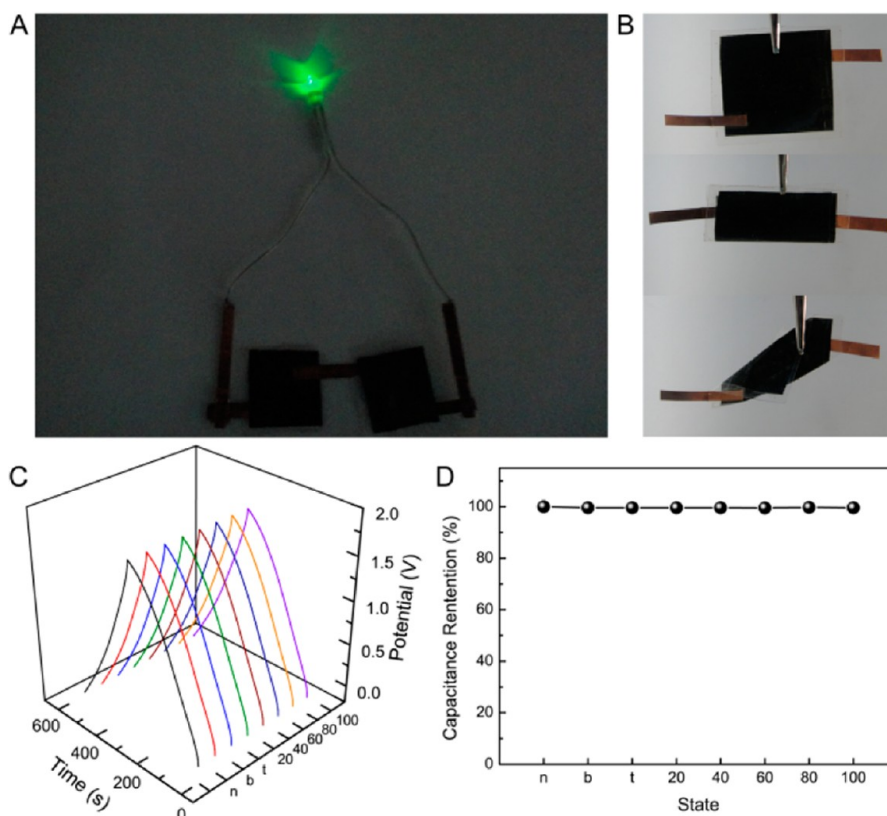
Figure 7. (A) A green light-emitting diode (LED) lighted by two asymmetric supercapacitors of CNTG-40//MG-50 connected in series. (B) Photographs of the asymmetric supercapacitor at normal, bending, and twisting states (from top to bottom). (C) Galvanostatic charge/discharge curves and (D) specific capacitance retention ratio of the asymmetric supercapacitor at normal (n), bending (b), and twisting (t) states and after being bent repeatedly (number of times indicated).

current density of 10 A/g, while the specific capacitance of rGO paper dramatically decreased to 45.3 F/g (Figure 3D). This higher rate capability of CNTG paper than rGO paper further confirms the introduction of CNTs between rGO layers improves the diffusion of electrolyte ions into the inner region of paper electrodes.

3.2. Positive Electrodes. Mn_3O_4 nanoparticles, exhibiting octahedral morphology with particle size of 50−100 nm, were synthesized by reacting $Mn(CH_3COO)_2 \cdot 4H_2O$ with NaOH (Figure 4A).[45] All the diffraction peaks in XRD pattern can be indexed to the tetragonal structure of Mn_3O_4 (Figure S4, Supporting Information). The pH_{pzc} (point of zero charge) of manganese oxides is about 2.25;[58] therefore, the prepared Mn_3O_4 nanoparticles have negatively charged surfaces with zeta-potential of −29 mV in neutral solutions and can form homogeneous dispersions with negatively charged rGO (Figure 4B). Mn_3O_4 nanoparticle/rGO (MG) papers with Mn_3O_4 mass ratio of 25% (MG-25) and 50% (MG-50) were successfully prepared by filtration of their mixture. Although a large amount of Mn_3O_4 nanoparticles were intercalated into rGO papers, the free-standing MG papers are still highly flexible (Figure 4C) and feature a multilayered structure throughout the entire cross-section, with Mn_3O_4 nanoparticles uniformly distributed between rGO nanosheets (Figure 4D,E,F). Such a sandwich structure is beneficial for buffering the volume changes of Mn_3O_4 nanoparticles during a continuous charge/discharge process. The incorporation of Mn_3O_4 nanoparticles can also minimize the restacking of rGO nanosheets, and consequently, the specific surface areas of MG-25 and MG-50 papers increased to 104.8 and 138.9 m^2/g, with their pore size distributions in the range of 2.0−8.0 nm (Figure S5, Supporting Information). Importantly, MG papers possess excellent mechanical stability even after loading large amounts of Mn_3O_4 nanoparticles. The tensile strengths of MG-50 and MG-25 papers are still as high as 24.0 and 31.9 MPa (Figure S3B, Supporting Information).

The all-solid-state symmetric supercapacitor of MG//MG, fabricated using the free-standing MG paper electrodes and the polymer gel electrolyte of PAAK/KCl, exhibits ideal capacitive behavior as evidenced by the nearly rectangular CV curves (Figure 5A) and the linear galvanostatic charge/discharge profiles (Figure 5B,C). The specific capacitances (C_{sc}) of MG-50 and MG-25 increased to 321.1 and 252.7 F/g at a current density of 0.5 A/g, much higher than that of rGO paper (99.7 F/g). The layered rGO nanosheets in MG papers can provide efficient charge transport channels with improved electrical conductivity and utilization efficiency of Mn_3O_4 nanoparticles,[59,60] leading to the paper electrodes with remarkable rate capability. Especially, when the current density increased to 10 A/g, the specific capacitance of MG-50 still can reach 243.6 F/g (Figure 5D).

3.3. All-Solid-State Asymmetric Supercapacitor. Taking advantage of the different stable potential windows of CNTG and MG paper electrodes (Figure 6A),[61] we fabricated an asymmetric supercapacitor of CNTG-40//MG-50 with the mass ratio of the two electrodes fixed to 0.85, which is based on their specific capacitance values and potential windows, in order to achieve a charge balance between the negative and positive electrodes.[62] As expected, the asymmetric supercapacitor can be cycled reversibly with a cell voltage up to 1.8 V in the polymer

gel electrolyte of PAAK/KCl (Figure 6B). The triangle shape of charge/discharge curves indicates the excellent capacitive behavior of the asymmetric supercapacitor in the whole potential range (Figure 6C). The specific capacitance (C_t) of CNTG-40//MG-50 can reach 72.6 F/g at a current density of 0.5 A/g and still retain 50.8 F/g at a higher current density of 10 A/g (Figure 6D). The asymmetric supercapacitor of CNTG-40//MG-50 possesses an energy density of 32.7 Wh/kg, which is much higher than that of the symmetric supercapacitors of CNTG-40//CNTG-40 (10.5 Wh kg^{-1}) and MG-50//MG-50 (7.1 Wh/kg) (Figure 6E). More importantly, when the power density increases to 9.0 kW/kg, the energy density of CNTG-40//MG-50 is still as high as 22.9 Wh/kg, suggesting that the asymmetric supercapacitor can provide a high energy density and a high power density concurrently. The asymmetric supercapacitor of CNTG-40//MG-50 also showed remarkable cycling stability and retained 86.0% of its initial capacitance after 10 000 cycles (Figure 6F).

We have also found that two asymmetric supercapacitors of CNTG-40//MG-50 connected in series can light a green light-emitting-diode, demonstrating its practical applications (Figure 7A). The maximum energy density (32.7 Wh/kg) of CNTG-40//MG-50 at the current density of 0.5 A/g is higher or comparable to the manganese oxides-based asymmetric super-capacitors in aqueous electrolytes reported previously, including activated carbon//mesoporous MnO_2 (10.4 Wh/kg at 0.3 A/g),[63] activated carbon//NaMnO$_2$ (19.5 Wh/kg at 0.04 A/g),[64] activated carbon//MnO_2 (17.3 Wh/kg at 0.55 A/g),[65] CNT//graphene-MnO_2 (12.5 Wh/kg at 0.45 A/g),[66] and graphene//graphene-MnO_2 (21.27 Wh/kg at 0.223 A/g).[67] Moreover, different from the supercapacitors packed with aqueous or organic electrolytes, the all-solid-state asymmetric supercapacitor of CNTG-40//MG-50 using the polymer gel electrolytes of PAAK/KCl exhibits excellent flexibility (Figure 7B). In addition, galvanostatic charge/discharge curves reveal that repeated bending and twisting had nearly no effect on the capacitive performance of the device (Figure 7C,D).

4. CONCLUSION

In conclusion, we fabricated flexible all-solid-state asymmetric supercapacitors with free-standing graphene composite paper electrodes and a polymer gel electrolyte. The flexible device, benefiting from the mechanical and electrical properties of graphene papers, the functionalities of CNTs and Mn_3O_4 nanoparticles, and the excellent electrochemical properties of polymer gel electrolyte, has demonstrated extraordinary performance for supercapacitor applications, such as signifi-cantly improved energy density and excellent cycling perform-ance. The integration of chemically tunable components of graphene, CNTs, functional nanoparticles, and polymer gel electrolytes opens the possibility for further screening of functional nanomaterials toward flexible and portable super-capacitors, batteries, fuel cells, biosensors, and other electronic devices.

■ ASSOCIATED CONTENT

ⓢ Supporting Information
Supplementary figures (Figure S1−S5). This information is available free of charge via the Internet at http://pubs.acs.org.

■ AUTHOR INFORMATION

Corresponding Author
*E-mail: hduan@ntu.edu.sg.

■ ACKNOWLEDGMENTS

■ REFERENCES

(1) Nyholm, L.; Nystrom, G.; Mihranyan, A.; Stromme, M. *Adv. Mater.* **2011**, *23*, 3751−3769.
(2) Gwon, H.; Kim, H. S.; Lee, K. U.; Seo, D. H.; Park, Y. C.; Lee, Y. S.; Ahn, B. T.; Kang, K. *Energy Environ. Sci.* **2011**, *4*, 1277−1283.
(3) Liu, F.; Song, S. Y.; Xue, D. F.; Zhang, H. J. *Adv. Mater.* **2012**, *24*, 1089−1094.
(4) Meng, C. Z.; Liu, C. H.; Chen, L. Z.; Hu, C. H.; Fan, S. S. *Nano Lett.* **2010**, *10*, 4025−4031.
(5) Kang, Y. J.; Chun, S. J.; Lee, S. S.; Kim, B. Y.; Kim, J. H.; Chung, H.; Lee, S. Y.; Kim, W. *ACS Nano* **2012**, *6*, 6400−6406.
(6) Yuan, L. Y.; Lu, X. H.; Xiao, X.; Zhai, T.; Dai, J. J.; Zhang, F. C.; Hu, B.; Wang, X.; Gong, L.; Chen, J.; Hu, C. G.; Tong, Y. X.; Zhou, J.; Wang, Z. L. *ACS Nano* **2012**, *6*, 656−661.
(7) Choi, B. G.; Hong, J.; Hong, W. H.; Hammond, P. T.; Park, H. *ACS Nano* **2011**, *5*, 7205−7213.
(8) Hall, P. J.; Mirzaeian, M.; Fletcher, S. I.; Sillars, F. B.; Rennie, A. J. R.; Shitta-Bey, G. O.; Wilson, G.; Cruden, A.; Carter, R. *Energy Environ. Sci.* **2010**, *3*, 1238−1251.
(9) Choudhury, N. A.; Sampath, S.; Shukla, A. K. *Energy Environ. Sci.* **2009**, *2*, 55−67.
(10) Pell, W. G.; Conway, B. E. *J. Power Sources* **2004**, *136*, 334−345.
(11) Long, J. W.; Belanger, D.; Brousse, T.; Sugimoto, W.; Sassin, M. B.; Crosnier, O. *MRS Bull.* **2011**, *36*, 513−522.
(12) Zhang, J. T.; Zhao, X. S. *ChemSusChem* **2012**, *5*, 818−841.
(13) Zhang, J. T.; Jiang, J. W.; Li, H. L.; Zhao, X. S. *Energy Environ. Sci.* **2011**, *4*, 4009−4015.
(14) Hu, L. B.; Chen, W.; Xie, X.; Liu, N. A.; Yang, Y.; Wu, H.; Yao, Y.; Pasta, M.; Alshareef, H. N.; Cui, Y. *ACS Nano* **2011**, *5*, 8904−8913.
(15) Bao, L. H.; Zang, J. F.; Li, X. D. *Nano Lett.* **2011**, *11*, 1215−1220.
(16) Zheng, G. Y.; Hu, L. B.; Wu, H.; Xie, X.; Cui, Y. *Energy Environ. Sci.* **2011**, *4*, 3368−3373.
(17) Wang, G. P.; Zhang, L.; Zhang, J. J. *Chem. Soc. Rev.* **2012**, *41*, 797−828.
(18) Frackowiak, E. *Phys. Chem. Chem. Phys.* **2007**, *9*, 1774−1785.
(19) Simon, P.; Gogotsi, Y. *Nat. Mater.* **2008**, *7*, 845−854.
(20) Wu, Q.; Xu, Y. X.; Yao, Z. Y.; Liu, A. R.; Shi, G. Q. *ACS Nano* **2010**, *4*, 1963−1970.
(21) Davies, A.; Audette, P.; Farrow, B.; Hassan, F.; Chen, Z. W.; Choi, J. Y.; Yu, A. P. *J. Phys. Chem. C* **2011**, *115*, 17612−17620.
(22) Sun, Y. Q.; Wu, Q.; Shi, G. Q. *Energy Environ. Sci.* **2011**, *4*, 1113−1132.
(23) Huang, Y.; Liang, J. J.; Chen, Y. S. *Small* **2012**, *8*, 1805−1834.
(24) Dai, L. M.; Chang, D. W.; Baek, J. B.; Lu, W. *Small* **2012**, *8*, 1130−1166.
(25) Yang, X. W.; Zhu, J. W.; Qiu, L.; Li, D. *Adv. Mater.* **2011**, *23*, 2833−2838.
(26) Xiao, F.; Song, J. B.; Gao, H. C.; Zan, X. L.; Xu, R.; Duan, H. W. *ACS Nano* **2012**, *6*, 100−110.
(27) Zhao, X.; Zhang, L. L.; Murali, S.; Stoller, M. D.; Zhang, Q. H.; Zhu, Y. W.; Ruoff, R. S. *ACS Nano* **2012**, *6*, 5404−5412.
(28) Lee, J. W.; Hall, A. S.; Kim, J. D.; Mallouk, T. E. *Chem. Mater.* **2012**, *24*, 1158−1164.
(29) Lu, X. H.; Zheng, D. Z.; Zhai, T.; Liu, Z. Q.; Huang, Y. Y.; Xie, S. L.; Tong, Y. X. *Energy Environ. Sci.* **2011**, *4*, 2915−2921.
(30) Zhao, X.; Hayner, C. M.; Kung, M. C.; Kung, H. H. *ACS Nano* **2011**, *5*, 8739−8749.

(31) Zhang, L. L.; Zhao, X.; Stoller, M. D.; Zhu, Y. W.; Ji, H. X.; Murali, S.; Wu, Y. P.; Perales, S.; Clevenger, B.; Ruoff, R. S. *Nano Lett.* **2012**, *12*, 1806−1812.

(32) Luo, J. Y.; Zhao, X.; Wu, J. S.; Jang, H. D.; Kung, H. H.; Huang, J. X. *J. Phys. Chem. Lett.* **2012**, *3*, 1824−1829.

(33) Chen, J.; Sheng, K. X.; Luo, P. H.; Li, C.; Shi, G. Q. *Adv. Mater.* **2012**, *24*, 4569−4573.

(34) Wu, Z. S.; Winter, A.; Chen, L.; Sun, Y.; Turchanin, A.; Feng, X.; Mullen, K. *Adv. Mater.* **2012**, *24*, 5130−5135.

(35) Wu, Z. S.; Ren, W. C.; Wang, D. W.; Li, F.; Liu, B. L.; Cheng, H. M. *ACS Nano* **2010**, *4*, 5835−5842.

(36) Chen, Z.; Augustyn, V.; Wen, J.; Zhang, Y. W.; Shen, M. Q.; Dunn, B.; Lu, Y. F. *Adv. Mater.* **2011**, *23*, 791−795.

(37) Xiao, F.; Li, Y. Q.; Zan, X. L.; Liao, K.; Xu, R.; Duan, H. W. *Adv. Funct. Mater.* **2012**, *22*, 2487−2494.

(38) Chen, P. C.; Shen, G. Z.; Shi, Y.; Chen, H. T.; Zhou, C. W. *ACS Nano* **2010**, *4*, 4403−4411.

(39) Choi, B. G.; Chang, S. J.; Kang, H. W.; Park, C. P.; Kim, H. J.; Hong, W. H.; Lee, S.; Huh, Y. S. *Nanoscale* **2012**, *4*, 4983−4988.

(40) Hummers, W. S.; Offeman, R. E. *J. Am. Chem. Soc.* **1958**, *80*, 1339−1339.

(41) Gao, H. C.; Xiao, F.; Ching, C. B.; Duan, H. W. *ACS Appl. Mater. Interfaces* **2011**, *3*, 3049−3057.

(42) Zhou, Y.; Bao, Q. L.; Tang, L. A. L.; Zhong, Y. L.; Loh, K. P. *Chem. Mater.* **2009**, *21*, 2950−2956.

(43) Gao, H. C.; Wang, Y. X.; Xiao, F.; Ching, C. B.; Duan, H. W. *J. Phys. Chem. C* **2012**, *116*, 7719−7725.

(44) Yu, A. P.; Su, C. C. L.; Roes, I.; Fan, B.; Haddon, R. C. *Langmuir* **2010**, *26*, 1221−1225.

(45) Hao, X. L.; Zhao, J. Z.; Li, Y. L.; Zhao, Y.; Ma, D. C.; Li, L. Z. *Colloids Surf., A: Physicochem. Eng. Aspects* **2011**, *374*, 42−47.

(46) Lee, K. T.; Wu, N. L. *J. Power Sources* **2008**, *179*, 430−434.

(47) Stoller, M. D.; Ruoff, R. S. *Energy Environ. Sci.* **2010**, *3*, 1294−1301.

(48) Brousse, T.; Toupin, M.; Belanger, D. *J. Electrochem. Soc.* **2004**, *151*, A614−A622.

(49) Gao, H. C.; Xiao, F.; Ching, C. B.; Duan, H. W. *ACS Appl. Mater. Interfaces* **2012**, *4*, 2801−2810.

(50) Park, S.; An, J. H.; Jung, I. W.; Piner, R. D.; An, S. J.; Li, X. S.; Velamakanni, A.; Ruoff, R. S. *Nano Lett.* **2009**, *9*, 1593−1597.

(51) Li, D.; Muller, M. B.; Gilje, S.; Kaner, R. B.; Wallace, G. G. *Nat. Nanotechnol.* **2008**, *3*, 101−105.

(52) Aboutalebi, S. H.; Chidembo, A. T.; Salari, M.; Konstantinov, K.; Wexler, D.; Liu, H. K.; Dou, S. X. *Energy Environ. Sci.* **2011**, *4*, 1855−1865.

(53) Huang, Z. D.; Zhang, B. A.; Oh, S. W.; Zheng, Q. B.; Lin, X. Y.; Yousefi, N.; Kim, J. K. *J. Mater. Chem.* **2012**, *22*, 3591−3599.

(54) Byon, H. R.; Lee, S. W.; Chen, S.; Hammond, P. T.; Shao-Horn, Y. *Carbon* **2011**, *49*, 457−467.

(55) Khan, U.; O'Connor, I.; Gun'ko, Y. K.; Coleman, J. N. *Carbon* **2010**, *48*, 2825−2830.

(56) Zhu, Y. W.; Murali, S.; Stoller, M. D.; Velamakanni, A.; Piner, R. D.; Ruoff, R. S. *Carbon* **2010**, *48*, 2118−2122.

(57) Wang, Y.; Shi, Z. Q.; Huang, Y.; Ma, Y. F.; Wang, C. Y.; Chen, M. M.; Chen, Y. S. *J. Phys. Chem. C* **2009**, *113*, 13103−13107.

(58) Murray, J. W. *J. Colloid Interface Sci.* **1974**, *46*, 357−371.

(59) Wang, G. K.; Sun, X.; Lu, F. Y.; Sun, H. T.; Yu, M. P.; Jiang, W. L.; Liu, C. S.; Lian, J. *Small* **2012**, *8*, 452−459.

(60) Cheng, Y. W.; Lu, S. T.; Zhang, H. T.; Varanasi, C. V.; Liu, J. *Nano Lett.* **2012**, *12*, 4206−4211.

(61) Fan, Z. J.; Yan, J.; Wei, T.; Zhi, L. J.; Ning, G. Q.; Li, T. Y.; Wei, F. *Adv. Funct. Mater.* **2011**, *21*, 2366−2375.

(62) Khomenko, V.; Raymundo-Pinero, E.; Frackowiak, E.; Beguin, F. *Appl. Phys. A: Mater. Sci. Process.* **2006**, *82*, 567−573.

(63) Wang, Y. T.; Lu, A. H.; Zhang, H. L.; Li, W. C. *J. Phys. Chem. C* **2011**, *115*, 5413−5421.

(64) Qu, Q. T.; Shi, Y.; Tian, S.; Chen, Y. H.; Wu, Y. P.; Holze, R. *J. Power Sources* **2009**, *194*, 1222−1225.

(65) Cottineau, T.; Toupin, M.; Delahaye, T.; Brousse, T.; Belanger, D. *Appl. Phys. A: Mater. Sci. Process.* **2006**, *82*, 599−606.

(66) Yu, G. H.; Hu, L. B.; Vosgueritchian, M.; Wang, H. L.; Xie, X.; McDonough, J. R.; Cui, X.; Cui, Y.; Bao, Z. N. *Nano Lett.* **2011**, *11*, 2905−2911.

(67) Deng, L. J.; Zhu, G.; Wang, J. F.; Kang, L. P.; Liu, Z. H.; Yang, Z. P.; Wang, Z. L. *J. Power Sources* **2011**, *196*, 10782−10787.